Optical Sectioning Deep Inside Live Embryos by Selective Plane Illumination Microscopy

Jan Huisken,* Jim Swoger, Filippo Del Bene, Joachim Wittbrodt, Ernst H. K. Stelzer*

Large, living biological specimens present challenges to existing optical imaging techniques because of their absorptive and scattering properties. We developed selective plane illumination microscopy (SPIM) to generate multidimensional images of samples up to a few millimeters in size. The system combines two-dimensional illumination with orthogonal camera-based detection to achieve high-resolution, optically sectioned imaging throughout the sample, with minimal photodamage and at speeds capable of capturing transient biological phenomena. We used SPIM to visualize all muscles in vivo in the transgenic Medaka line Arnie, which expresses green fluorescent protein in muscle tissue. We also demonstrate that SPIM can be applied to visualize the embryogenesis of the relatively opaque *Drosophila melanogaster* in vivo.

Modern life science research often requires multidimensional imaging of a complete spatiotemporal pattern of gene and protein expression or tracking of tissues during the development of an intact embryo (*1*). In order to visualize the precise distribution of developmental events such as activation of specific genes, a wide range of processes, from small-scale (subcellular) to large-scale (millimeters), needs to be followed. Ideally, such events, which can last from seconds to days, will be observed in live and fully intact embryos.

Several techniques have been developed that allow mapping of the three-dimensional (3D) structure of large samples (*2*). Gene expression has been monitored by in situ hybridization and block-face imaging (*3*). Techniques that provide noninvasive (optical) sectioning, as opposed to those that destroy the sample, are indispensable for live studies. Optical projection tomography can image fixed embryos at high resolution (*4*). Magnetic resonance imaging (*5*) and optical coherence tomography (*6*) feature noninvasive imaging, but do not provide specific contrasts easily.

In optical microscopy, green fluorescent protein (GFP) and its spectral variants are used for high-resolution visualization of protein localization patterns in living organisms (*7*). When GFP-labeled samples are viewed, optical sectioning (which is essential for its elimination of out-of-focus light) is obtainable by laser scanning microscopy (LSM),
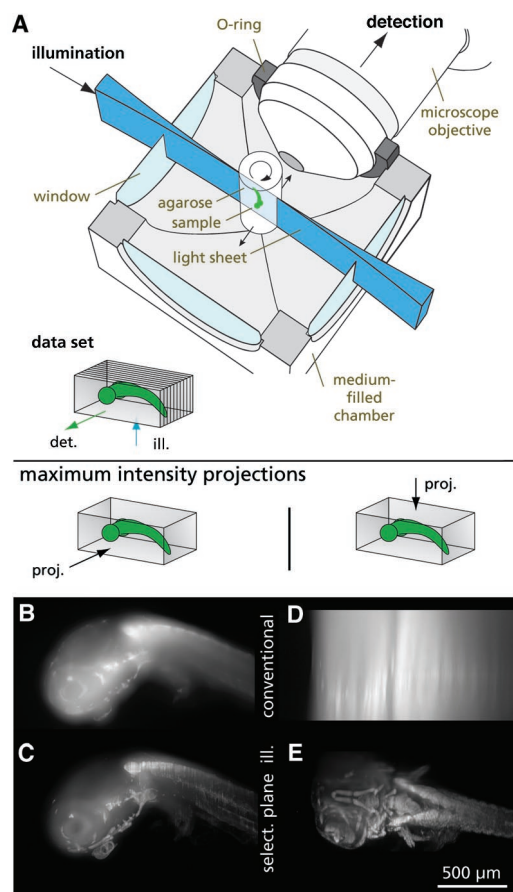
either by detection through a pinhole (confocal LSM) (*8*) or by exploitation of the nonlinear properties of a fluorophore (multiphoton microscopy) (*9*). Despite the improved resolution, LSM suffers from two major limitations: a limited penetration depth in heterogeneous samples and a marked difference between the lateral and axial resolution.

We developed selective plane illumination microscopy (SPIM), in which optical sectioning is achieved by illuminating the sample along a separate optical path orthogonal to the detection axis (Fig. 1 and fig. S1). A similar approach in confocal theta microscopy has been demonstrated to improve axial resolution (*10–12*). In SPIM, the excitation light is focused by a cylindrical lens to a sheet of light that illuminates only the focal plane of the detection optics, so that no out-of-focus fluorescence is generated (optical sectioning). The net effect is similar to that achieved by confocal LSM. However, in SPIM, only the plane currently observed is illuminated and therefore affected by bleaching. Therefore, the total number of fluorophore excitations required to image a 3D sample is greatly reduced compared to the number in confocal LSM (supporting online text).

GFP-labeled transgenic embryos of the teleost fish Medaka (*Oryzias latipes*) (*13*) were imaged with SPIM. In order to visu-

Fig. 1. (A) Schematic of the sample chamber. The sample is embedded in a cylinder of agarose gel. The solidified agarose is extruded from a syringe (not shown) that is held in a mechanical translation and rotation stage. The agarose cylinder is immersed in an aqueous medium that fills the chamber. The excitation light enters the chamber through a thin glass window. The microscope objective lens, which collects the fluorescence light, dips into the medium with its optical axis orthogonal to the plane of the excitation light. The objective lens is sealed with an O-ring and can be moved axially to focus on the plane of fluorescence excited by the light sheet. In a modified setup, for low-magnification lenses not corrected for water immersion, a chamber with four windows and no O-ring can be used. In this case, the objective lens images the sample from outside the chamber. det., detection; ill., illumination; proj., projection. **(B to E)** A Medaka embryo imaged with SPIM by two different modes of illumination. Lateral [(B) and (C)] and dorsal-ventral [(D) and (E)] maximum projections are shown. In (B) and (D), the sample was illuminated uniformly, i.e., without the cylindrical lens, as with a conventional widefield microscope. There is no optical sectioning. The elongation of fluorescent features along the detection axis is clearly visible in (D). In contrast, selective (select.) plane illumination [(C) and (E)] provided optical sectioning because the cylindrical lens focused the excitation light to a light sheet. Both image stacks were taken with a Zeiss Fluar 5×, 0.25 objective lens.

European Molecular Biology Laboratory (EMBL), Meyerhofstraße 1, D-69117 Heidelberg, Germany.

*To whom correspondence should be addressed. E-mail: huisken@embl.de (J.H.) and stelzer@embl.de (E.H.K.S.)

alize the internal structure, we imaged the transgenic line Arnie, which expresses GFP in somatic and smooth muscles as well as in the heart (*14*). A 4-day-old fixed Arnie embryo [stage 32 (*15*)] is shown in Fig. 1. SPIM was capable of resolving the internal structures of the entire organism with high resolution (better than 6 μm) as deep as 500 μm inside the fish, a penetration depth that cannot be reached using confocal LSM (fig. S6). The axial resolution in SPIM is determined by the lateral width of the light sheet; for the configuration shown in Fig. 1, the axial extent of the point spread function (PSF) was about 6 μm, whereas without the light sheet it was more than 20 μm (supporting online text).

Any fluorescence imaging system suffers from scattering and absorption in the tissue; in large and highly scattering samples, the image quality decreases as the optical path length in the sample increases. This problem can be reduced by a multiview reconstruction, in which multiple 3D data sets of the same object are collected from different directions and combined in a postprocessing step (*16–18*). The high-quality information is extracted from each data set and merged into a single, superior 3D image (supporting online text). One way to do this is by parallel image acquisition, using more than one lens for the detection of fluorescence (*18*).

We collected SPIM data for a multiview reconstruction sequentially by generating multiple image stacks between which the sample was rotated. Sample deformations were avoided with a rotation axis parallel to gravity (Fig. 1). In contrast to tomographic reconstruction techniques [such as those in (*4*)], which require extensive processing of the data to yield any meaningful 3D information, rotation and subsequent data processing are optional in SPIM. They allow a further increase in image quality and axial resolution compared to a single stack, but in many cases a single, unprocessed 3D SPIM stack alone provides sufficient information.

We performed a multiview reconstruction with four stacks taken with four orientations of the same sample (figs. S2 and S3). Combination of these stacks (supporting online text) yielded a complete view of the sample, ~1.5 mm long and ~0.9 mm wide. In Fig. 2, the complete fused data set is shown and the most pronounced tissues are labeled. The decrease in image quality with penetration depth is corrected by the fusion process. It yielded an increased information content in regions that were obscured (by absorption or scattering in the sample) in some of the unprocessed single views.

The method of embedding the sample in a low-concentration agarose cylinder is nondisruptive and easily applied to live embryos. We routinely image live Medaka and *Drosophila* embryos over periods of up to 3 days without detrimental effects on embryogenesis and development. To demonstrate the potential of SPIM technology, we investigated the Medaka heart, a structure barely accessible by conventional confocal LSM because of its ventral position in the yolk cell. We imaged transgenic Medaka Arnie embryos and show a reconstruction of the inner heart surface (Fig. 3A) derived from the data set shown in Fig. 2. This reveals the internal structure of the heart ventricle and atrium. In a slightly earlier stage, internal organs such as the heart and other mesoendodermal deriva-
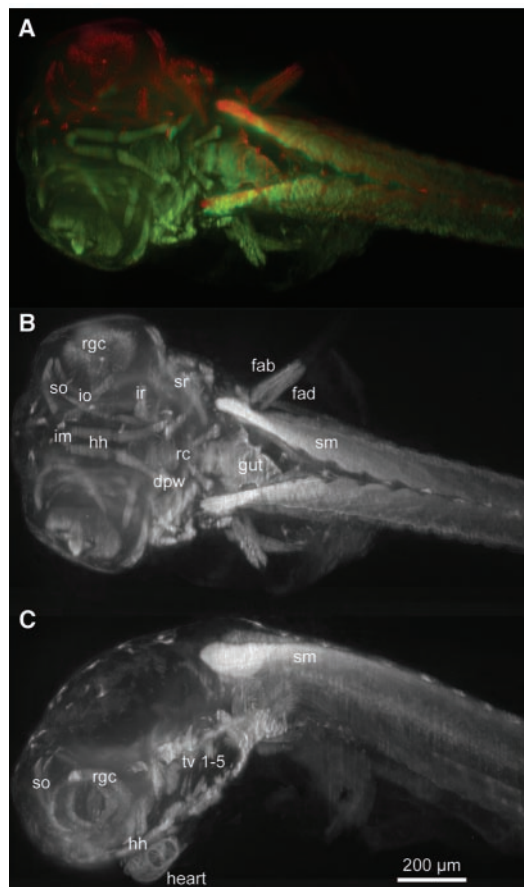
Fig. 2. A Medaka embryo (the same as in Fig. 1) imaged with SPIM and processed by multiview reconstruction (figs. S2, S3, and S6 and movies S1 and S2). (**A**) Overlay of a single stack (green) and the fusion of four data sets (red and green). (**B**) Dorsal-ventral and (**C**) lateral maximum intensity projections of the fused data. The high resolution throughout the entire fish allows identification of different tissues: rgc, retinal ganglion cells; so, superior oblique; io, inferior oblique; ir, inferior rectus; sr, superior rectus; im, intermandibualaris; hh, hyohyal; rc, rectus communis; dpw, dorsal pharyngeal wall; fad, fin adductor; fab, fin abductor; sm, somitic mesoderm; tv, transverse ventrals. The stack has a size of 1201 by 659 by 688 pixels (1549 μm by 850 μm by 888 μm).

Fig. 3. A Medaka heart imaged with SPIM (movies S3 and S4). (**A**) Surface rendering of the heart taken from the data shown in Fig. 2. The heart has been cut open computationally to make the internal structure visible. hv, heart ventricle; ha, heart atrium. (**B**) Schematic representation of a Medaka embryo at stage 26 of development (*13*), 2 days post-fertilization. Three optically sectioned planes are indicated. At this stage, ventral structures such as the heart are deeply buried in the yolk sphere. d, dorsal; v, ventral; a, anterior; p, posterior; y, yolk; ey, eye. (**C**) Optical section of an Arnie embryo showing the eye and the optic nerve labeling and the dorsal part of the heart ventricle. on, optic nerve. (**D**) Optical section showing the heart ventricle chamber and the dorsal wall of the heart atrium. (**E**) Optical section showing the atrium chamber.
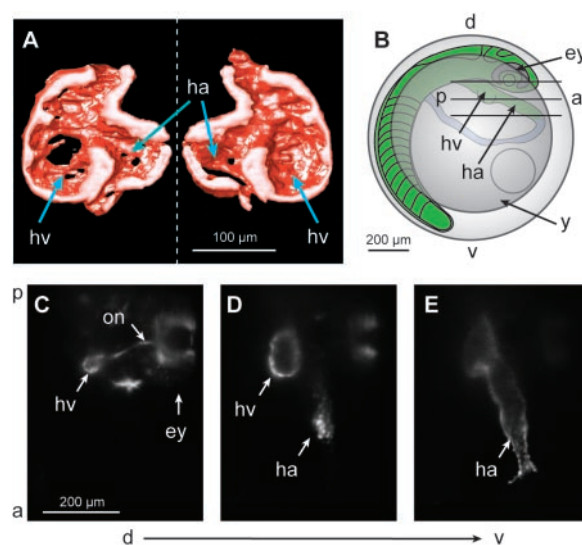
tives are deeply buried in the yolk sphere, under the body of the embryo (Fig. 3B). In Fig. 3, C to E, three optical sections at different depths illustrate GFP expression in the muscles of the living heart. Fast frame recording (10 frames per s) allows imaging of the heartbeat (movies S3 and S4); similar imaging has previously only been demonstrated at stages when the heart is exposed and by cooling the embryo to reduce the heart rate (*19*).

To demonstrate that SPIM can also be used to image the internal structures of relatively opaque embryos, we recorded a time series (movie S5) of the embryogenesis of the fruit fly *Drosophila melanogaster* (Fig. 4). GFP-moesin labeled the plasma membrane throughout the embryo (*20*). Even without multiview reconstruction, structures inside the embryo are clearly identifiable and traceable. Stacks (56 planes each) were taken automatically every 5 min over a period of 17 hours, without refocusing or realignment. Even after being irradiated for 11,480 imag-

es, the embryo was unaffected and completed embryogenesis normally.

In summary, we present an optical wide-field microscope capable of imaging protein expression patterns deep inside both fixed and live embryos. By selective illumination of a single plane, the excitation light is used efficiently to achieve optical sectioning and reduced photodamage in large samples, key features in the study of embryonic development. The method of sample mounting allows positioning and rotation to orient the sample for optimal imaging conditions. The optional multiview reconstruction combines independently acquired data sets into an optimal representation of the sample. The implementation of other contrasts such as scattered light will be straightforward. The system is compact, fast, optically stable, and easy to use.

SPIM is well suited for the visualization of high-resolution gene and protein expression patterns in three dimensions in the

context of morphogenesis. Heart function and development can be precisely followed in vivo using SPIM in Arnie transgenic embryos. Because of its speed and its automatable operation, SPIM can serve as a tool for large-scale studies of developing organisms and the systematic and comprehensive acquisition and collection of expression data. Even screens for molecules that interfere with development and regeneration on a medium-throughput scale seem feasible. SPIM technology can be readily applied to a wide range of organisms, from whole embryos to single cells. Subcellular resolution can be obtained in live samples kept in a biologically relevant environment within the organism or in culture. Therefore, SPIM also has the potential to be of use in the promising fields of 3D cultured cells (*21*) and 3D cell migration (*22*).

References and Notes

1. S. G. Megason, S. E. Fraser, *Mech. Dev.* **120**, 1407 (2003).
2. S. W. Ruffins, R. E. Jacobs, S. E. Fraser, *Curr. Opin. Neurobiol.* **12**, 580 (2002).
3. W. J. Weninger, T. Mohun, *Nature Genet.* **30**, 59 (2002).
4. J. Sharpe et al., *Science* **296**, 541 (2002).
5. A. Y. Louie et al., *Nature Biotechnol.* **18**, 321 (2000).
6. D. Huang et al., *Science* **254**, 1178 (1991).
7. M. Chalfie, Y. Tu, G. Euskirchen, W. W. Ward, D. C. Prasher, *Science* **263**, 802 (1994).
8. J. B. Pawley, *Handbook of Biological Confocal Microscopy* (Plenum, New York, 1995).
9. W. Denk, J. H. Strickler, W. W. Webb, *Science* **248**, 73 (1990).
10. E. H. K. Stelzer, S. Lindek, *Opt. Commun.* **111**, 536 (1994).
11. E. H. K. Stelzer et al., *J. Microsc.* **179**, 1 (1995).
12. S. Lindek, J. Swoger, E. H. K. Stelzer, *J. Mod. Opt.* **46**, 843 (1999).
13. J. Wittbrodt, A. Shima, M. Schartl, *Nature Rev. Genet.* **3**, 53 (2002).
14. Materials and methods are available as supporting material on *Science* Online.
15. T. Iwamatsu, *Zool. Sci.* **11**, 825 (1994).
16. P. J. Shaw, *J. Microsc.* **158**, 165 (1990).
17. S. Kikuchi, K. Sonobe, S. Mashiko, Y. Hiraoka, N. Ohyama, *Opt. Commun.* **138**, 21 (1997).
18. J. Swoger, J. Huisken, E. H. K. Stelzer, *Opt. Lett.* **28**, 1654 (2003).
19. J. R. Hove et al., *Nature* **421**, 172 (2003).
20. K. A. Edwards, M. Demsky, R. A. Montague, N. Weymouth, D. P. Kiehart, *Dev. Biol.* **191**, 103 (1997).
21. A. Abbott, *Nature* **424**, 870 (2003).
22. D. J. Webb, A. F. Horowitz, *Nature Cell Biol.* **5**, 690 (2003).
23. We thank S. Enders and K. Greger for contributions to the instrumentation and F. Jankovics and D. Brunner for providing the *Drosophila* samples. The beating-heart data was recorded by K. Greger.
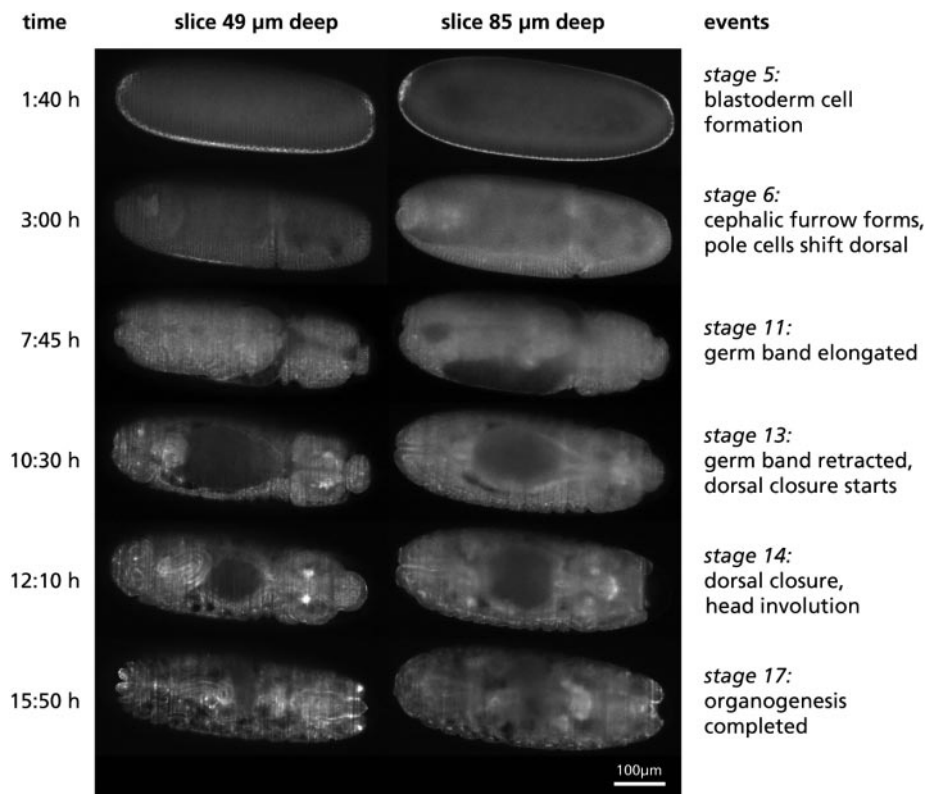
Fig. 4. Time-lapse imaging of *Drosophila melanogaster* embryogenesis. Six out of 205 time points acquired are shown (movie S5). At each time point, 56 planes were recorded, from which two (at depths of 49 μm and 85 μm below the cortex) are shown. No multiview reconstruction was necessary. The optical sectioning capability and the good lateral resolution are apparent. Despite the optically dense structure of the *Drosophila* embryo, features are well resolved at these depths in the sample. For this figure, the images were oriented so that the illumination occurs from below. This results in a slight drop in intensity and clarity from the bottom to the top of each slice. Nevertheless, the information content across the embryo is nearly uniform, and the overall morphogenetic movements during embryonic development can be followed. The images were normalized to exhibit the same overall intensity, thus compensating the continuous production of GFP-moesin. We took 205 stacks at 5-min intervals with a Zeiss Achroplan 10×, 0.30W objective lens (56 planes per stack at 4-μm spacing) for 11,480 images in total.